PAPER

Check for updates

Enhanced visible light photocatalytic activity of BiOBr by *in situ* reactable ionic liquid modification for pollutant degradation

Zhidong Wei, Ruishuo Li and Rui Wang (ID)*

In this study, hierarchical BiOBr microspheres were synthesized *via* a one-pot solvothermal method in the presence of imidazole ionic liquids. The resultant samples were characterized by XRD, SEM, HRTEM, PL, EPR, EIS and UV-vis absorption spectroscopy. The photoactivity of BiOBr was evaluated by the photocatalytic degradation of methyl orange (MO) and tetracycline hydrochloride. Oxygen vacancies were detected in the system and proven to be correlated with the activity of the catalyst. It was also revealed that BiOBr microspheres prepared by 1-butyl-3-methylimidazolium bromide at 433 K for 8 hours displayed a superior performance compared to the other samples in the degradation of model organic contaminants. After 4.5 hours of reaction, the highest degradation efficiency of 94.0% was achieved by BiOBr-C$_4$-Br. Stronger photoluminescence spectral intensities could be obtained as the cationic chain lengths of the ionic liquids reduced gradually. According to our experiments, the better performance of BiOBr-C$_4$-Br in the degradation of model pollutants can be attributed to the effect of oxygen vacancies. The findings of our work may have important implications for the design of BiOBr.

1. Introduction

As a promising state-of-the-art photocatalyst, TiO$_2$ has ignited extensive scientific interest since it was first reported in 1972,[1] due to its strong oxidizing ability, low toxicity, low cost and facile synthesis. Being regarded as an effective photocatalytic semiconductor material, TiO$_2$ was applied for solar energy conversion and for solving environmental problems.[2-6] Although it has been widely used, TiO$_2$ still has the limitation that it can only absorb ultraviolet light. As we all know, ultraviolet light represents merely 4% of the solar energy available, whereas visible light accounts for 43% of the solar spectrum. Consequently, it has become a hot topic to explore catalysts with visible-light-response capability.[7]

Recently, BiOBr has attracted our attention because the hybridization between the O$_{2p}$ and Bi$_{6s}$ states narrows the band gap well and enables BiOBr to make use of visible light.[8] In addition, it has good chemical stability and is environmentally friendly.[9,10] BiOBr, which has [Bi$_2$O$_2$] layer structures interleaved by double slabs of halogen atoms, is a transcendental V–VI–VII ternary semiconductor. Several researchers have reported on the applications and preparation of BiOBr micro/nanostructures. Deng *et al.* reported the synthesis of one-dimensional (1D) BiOBr nanowires and nanotubes using the cationic surfactant cetyltrimethylammonium bromide (CTAB) as the bromine source.[11] Two-dimensional (2D) single-

crystalline BiOBr nanoplates, nanosheets and microsheets were also obtained by hydrogen peroxide oxidation of bulk metal Bi particles in a surfactant-mediated solution.[12] Fabrication of three-dimensional (3D) BiOBr materials are more sophisticated. Xia *et al.* successfully synthesized 3D flower-like hollow microsphere and porous nanosphere structures through a one-pot ethylene glycol (EG)-assisted solvothermal process in the presence of a reactable ionic liquid (IL).[13] Moreover, the applications of 3D BiOBr have been reported by many researchers. Zhang *et al.* applied BiOBr microspheres for the adsorption of methyl blue (MB) and Cr(VI).[14] Jiang *et al.* designed flake-like BiOBr using an acetic acid (HAc)-assisted hydrothermal route for photocatalytic degradation of methyl orange (MO).[15] Mesoporous BiOBr microspheres were collected by Feng and coworkers through a facile solvothermal method, and the activity of the catalyst in toluene photodecomposition was explored.[16] Ai and co-workers found that BiOBr microspheres, which displayed efficient photocatalytic activity, could remove the textile NO species in indoor air.[17]

ILs are non-volatile and non-flammable organic salts with low melting points.[14] Because of their unique properties, such as extremely low volatility, high ionic conductivity, good dissolving ability and designable structures, they have been widely used as solvents, templates, and reactants for the synthesis of inorganic nanomaterials.[18-21] In 2000, Dai and co-workers first observed the construction of a SiO$_2$ aerogel which exhibited superior capability for solvation *via* a method using ILs.[7] Zhang's groups found that IL modification could trap the photoexcited electron in the conduction band of BiOI to inhibit

School of Environmental Science and Engineering, Shandong University, No. 27 Shanda South Road, Jinan 250199, P. R. China. E-mail: ree_wong@hotmail.com

the recombination of photoinduced electron–hole pairs, and thus enhance the photocatalytic activity of BiOI in the degradation of organic pollutants.[18] Xia and co-workers have also prepared carbon quantum dot/BiOBr nanoplates *via* an IL-assisted hydrothermal approach. The synthesized catalyst possessed highly efficient photocatalytic activity for three different kinds of pollutant under visible light.[22] In addition, other nanomaterials have been prepared in ILs, including Au nanosheets,[23] high-quality TiO_2 nanocrystals,[24] rod-like, star-like and flower-like ZnO nanostructures,[25] $CuCl_2$ nanoplates,[26] ZnSe hollow nanospheres[27] and so forth. In these works, ILs acted not only as solvents, but also as templates. Nevertheless, the full potential of ILs as reagents in the controllable synthesis of BiOBr nanostructures remains to be fully explored.

Although there have been some achievements in the IL-assisted preparation of BiOBr, it is necessary to develop a more ecofriendly and convenient synthesis method for BiOBr. Hence, the synthetic conditions still need to be explored. Furthermore, it is of great practical relevance to promote the photocatalytic performance of BiOBr by exploring the conditions for material synthesis. In our work, we synthesized BiOBr nanomaterials *via* an IL-assisted hydrothermal approach to determine the best preparation conditions. BiOBr samples were prepared using different kinds of ILs, and it was demonstrated that a type of imidazole IL could significantly influence the visible light photocatalytic activity of BiOBr.

2. Experimental section

2.1 Materials and reagents

Bismuth nitrate pentahydrate ($Bi(NO_3)_3 \cdot 5H_2O$) was obtained from Tianjin Bodi Chemical Co. Ltd; dry ethanol and glycol ether were bought from Tinjin Fuyu Chemical Co. Ltd; ILs were purchased from Shanghai Chengjie Co. Ltd. All of the chemicals were of analytical grade and were used as received without further purification.

2.2 Synthesis methods

At first, the optimum conditions of reaction time and temperature were explored. After this was successfully completed, BiOBr particles were prepared with ILs. The procedure can be summarized as follows: 2 mmol of bismuth nitrate pentahydrate was dissolved in 10 mL of GE. This was marked as solution A. In another process, solution B was formed by the dissolution of 2 mmol of 1-butyl-3-methylimidazolium bromide in 20 mL of GE. Solutions A and B were mixed together drop by drop with continuous stirring. When the colour of the solution turned from yellow green to clear (the BiOBr precursor solution was formed), 1 mmol of 1-butyl-3-methylimidazolium bromide was introduced. After stirring for another 1 h, the mixture was transferred into a 50 mL Teflon reactor inside a high pressure vessel and heated at 433 K for 8 h. The resulting precipitates were collected, and thoroughly washed with deionized water and ethanol three times. After drying at 353 K in the air, the products were obtained. The particles were denoted as BiOBr-C_4-Br. BiOBr was then synthesized by ILs with different chain

lengths using the same procedure except that 1-butyl-3-methylimidazolium bromide was substituted by 1-octyl-3-methylimidazolium bromide, 1-dodecyl-3-methylimidazolium bromide and 1-cetyl-3-methylimidazolium bromide in solution B and in the addition to the clear BiOBr precursor. The products were denoted as BiOBr-C_8, BiOBr-C_{12} and BiOBr-C_{16}, separately.

BiOBr was modified by ILs with different kinds of anions *via* a similar procedure. After the mixture of solution A and B had turned clear, 1 mmol of 1-butyl-3-methylimidazolium tetra-fluoroborate or 1-butyl-3-methyl-imidazole hexa-fluorophosphate was introduced. Other steps were the same as those used in the preparation of BiOBr-C_4-Br. The resulting products were BiOBr-BF_4 and BiOBr-PF_6.

2.3 Characterization

X-ray powder diffraction (XRD) analysis was recorded with a Bruker Advance D8 powder diffractometer with a Cu-Kα radiation source. The scan range was 10–80° with a rate of 0.02° s^{-1}. The morphologies of the BiOBr catalysts were observed using scanning electron microscopy (SEM) and high resolution transmission electron microscopy (HRTEM) (JEOL JEM-2100F, accelerating voltage 200 kV). The Brunauer–Emmett–Teller (BET) specific surface areas of the samples were measured with a physical absorption analyzer (Tristar 3020). UV-vis diffuse reflectance spectra (DRS) were obtained at room temperature between 200 and 800 nm using a UV-vis spectrophotometer (UV-4100, Hitachi, Japan) with $BaSO_4$ as a reflectance standard. To study the recombination of photoinduced charge carriers, photoluminescence (PL, Hitachi F-4500, 250 nm) spectra were collected. Electron paramagnetic resonance (EPR) tests were carried out in a magnetic field modulation of 100 kHz using a Bruker ER 200-SRC spectrometer at 77 K. Electrochemical impedance spectra (EIS) were analyzed by an electrochemical system (CHI-660D, China).

2.4 Photocatalytic activity measurement

The photocatalytic activities of the as-prepared BiOBr samples were tested by their performance in the photodegradation of methyl orange (MO) and tetracycline hydrochloride. Experiments were carried out in a photocatalytic reactor irradiated by a 300 W Xenon lamp with a 420 nm UV light cut filter. In a typical procedure, 0.1 g BiOBr photocatalyst were added into 100 mL solution with a MO concentration of 10 mg L^{-1}. Prior to the photocatalytic reaction, the suspension was magnetically stirred for 30 min in the dark to reach an adsorption–desorption equilibrium. Then the mixture was exposed to light irradiation under magnetic stirring. At certain intervals, about 4 mL of the suspension was sampled and filtered to remove the photocatalyst. The supernatant solution was analyzed by the UV spectrophotometer. The original concentration of the MO was represented by C_1.

3. Results and discussion

The phase and purity of the samples was measured by XRD. Fig. 1 shows the typical diffraction patterns of the as-
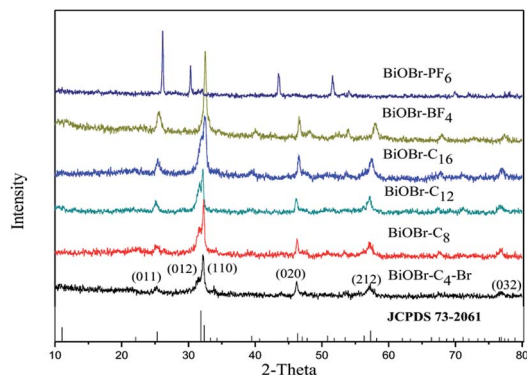
Fig. 1 XRD patterns for BiOBr samples prepared by different kinds of ionic liquids.

synthesized BiOBr samples. All the peaks of the as-prepared BiOBr samples at 25.3° (011), 31.8° (012), 32.3° (110), 46.3° (020), 57.3° (212) and 76.7° (032) were readily indexed to the tetragonal phase of BiOBr whose lattice parameters are $a = 0.3915$ nm and $c = 0.8076$ nm (space group: $P4/nmm$, JCPDS card no. 73-2061). This indicates that the BiOBr catalysts were synthesized successfully. Furthermore, the samples synthesized by 1-butyl-3-methylimidazolium bromide were also characterized by SEM and HRTEM, as exhibited in Fig. 2. It can be observed from the SEM images that BiOBr-C$_4$-Br formed aggregated, tremella-ball-like structures, which was in good agreement with the BiOBr reported previously.[13] The surfaces of the samples were comprised of numerous layered-crosslinked BiOBr, which was different from the traditional layered BiOBr
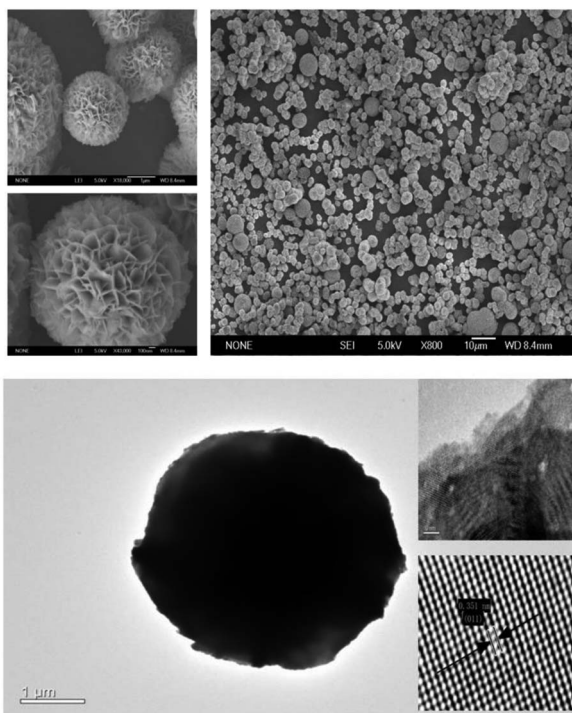

Fig. 2 SEM and HRTEM images of BiOBr-C$_4$-Br synthesized by ionic liquids.

synthesized by NaBr or KBr. This special morphology could make full use of the light, which might be due to the multiple reflections among the layered-crosslinked appearance. To gain a better understanding of the microstructure of the as-synthesized microspheres, the BiOBr-C$_4$-Br samples were analyzed by HRTEM. The HRTEM image showed that the lattice spacing (0.351 nm) matched the (011) crystal facet of BiOBr. It can be concluded that the BiOBr nanosheets were assembled to form microflower-like morphologies and structures along the (011) planes, and that BiOBr microflowers of 2–4 μm in size were obtained. From these results, we could conclude that BiOBr had been successfully prepared with different kinds of ILs, including 1-butyl-3-methylimidazolium bromide. In the procedure for the BiOBr preparation, the ILs played not only the role of the bromide source, but also the roles of the template and the solvent.

UV-vis diffuse reflectance spectroscopy was conducted to measure the optical properties of the BiOBr samples. The band gap energy (E_g) of BiOBr prepared with different kinds of ILs can be estimated according to eqn (1) and the graph is exhibited in Fig. 3(b).

$$ah\nu = k(h\nu - E_g)^{1/n} \qquad (1)$$

where k represents a constant, and a, h, ν and E_g are the absorption coefficient, Plank constant, light frequency, and band gap, respectively.[28] Among them, n depends on the characteristics of the transition in a semiconductor. For BiOBr, the value of n is 2 because it is an indirect transition semiconductor, whereas a direct transition semiconductor has an n value of 0.5. The intercepts of the tangents at the x-axis give a good approximation of the band gap energies (E_g). The E_g values of the synthesized BiOBr samples could thus be estimated from plots of $(ah\nu)^{1/2}$ *versus* photo energy ($h\nu$). As can be seen from Fig. 3, by extrapolating the linear region, the band gap energies of BiOBr-C$_4$-Br, BiOBr-C$_8$, BiOBr-C$_{12}$, BiOBr-C$_{16}$, BiOBr-BF$_4$ and BiOBr-PF$_6$ were calculated to be 2.31, 2.30, 2.27, 2.21, 2.16, 1.97 eV, respectively, as listed in Table 1. Moreover, those as-prepared catalysts have appropriate band gaps for activation by visible light for the photocatalytic degradation of organic pollutants, as manifested in Fig. 3(a).

MO was selected as the model contaminant for preliminary evaluation of the photocatalytic activities of the samples. The photocatalytic performances of the BiOBr samples were measured by evaluating the maximum absorption intensity of the MO chromophoric group at the maximum wavelength of 463 nm under a Xe lamp with a 420 nm UV light cut filter. As shown in Fig. 4(a) and (b), it can be found that the degradation of MO by BiOBr-C$_4$-Br reached 94.0% in 270 min, which was more efficient than that of BiOBr-C$_8$ (85.1%), BiOBr-C$_{12}$ (83.5%), BiOBr-C$_{16}$ (69.2%), BiOBr-BF$_4$ (66.8%) and BiOBr-PF$_6$ (23.7%) under the same conditions.

To get a better understanding of the reaction kinetics of the MO degradation catalyzed by the as-prepared BiOBr photocatalysts, the experimental data were fitted by a first-order model as expressed by eqn (2); the value of the rate constant k usually acts as an indication of the activity of the photocatalysts.
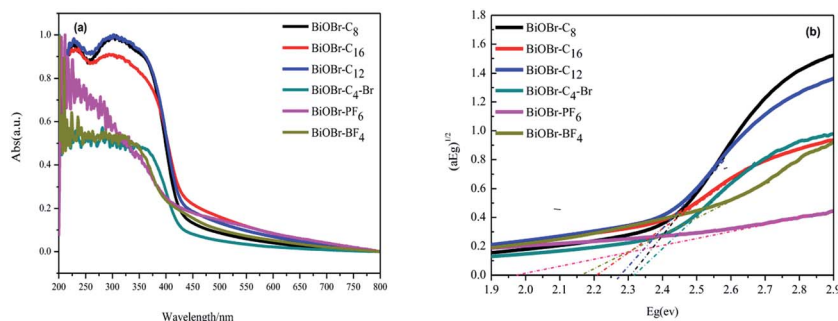
$$-\ln(C/C_1) = kt \qquad (2)$$

Fig. 3   (a) UV-vis absorption spectra and (b) band energy plots of BiOBr synthesized by ionic liquids.

Table 1 Band energy, reaction rate and proportion of (011) facets of BiOBr synthesized by ionic liquids

Samples	E_g (eV)	Reaction rate (min^{-1})	(011) Facets (%)
BiOBr-C$_4$-Br	2.31	0.0098	2.9
BiOBr-C$_8$	2.30	0.0058	3.8
BiOBr-C$_{12}$	2.27	0.0047	5.5
BiOBr-C$_{16}$	2.23	0.0039	6.7
BiOBr-BF$_4$	2.16	0.0023	7.8
BiOBr-PF$_6$	1.97	0.0008	9.6

C_1 and C are the initial concentration of MO and the apparent concentration of MO after degradation, respectively. Moreover, k is the kinetic rate constant. The values of k were obtained from the slope and the intercept of the linear plot. Fig. 4(b) exhibits a linear relationship between $\ln(C/C_1)$ and the irradiation time for MO degradation. As can be seen from Fig. 4(b) and Table 1, BiOBr-C$_4$-Br exhibited the highest rate constant (0.0111 min^{-1}) for MO photodegradation, whereas other samples were 0.0058 min^{-1}, 0.0047 min^{-1}, 0.0039 min^{-1}, 0.0023 min^{-1} and 0.0008 min^{-1}. From the aspect of the chain length of the ILs, it can be found that both the photocatalytic rate and the degradation efficiency of the MO decreased as the chain length of the IL increased. On the other hand, from the aspect of the anions of the ILs, BiOBr-C$_4$-Br exhibited a better degradation rate than the BiOBr synthesized by the 1-butyl-3-methylimidazolium tetrafluoroborate or the 1-butyl-3-methyl-imidazole hexafluorophosphate. In addition, the photocatalytic rate followed the same trend. However, dyes can absorb visible light and act as photosensitizers which will obscure the intrinsic activity of
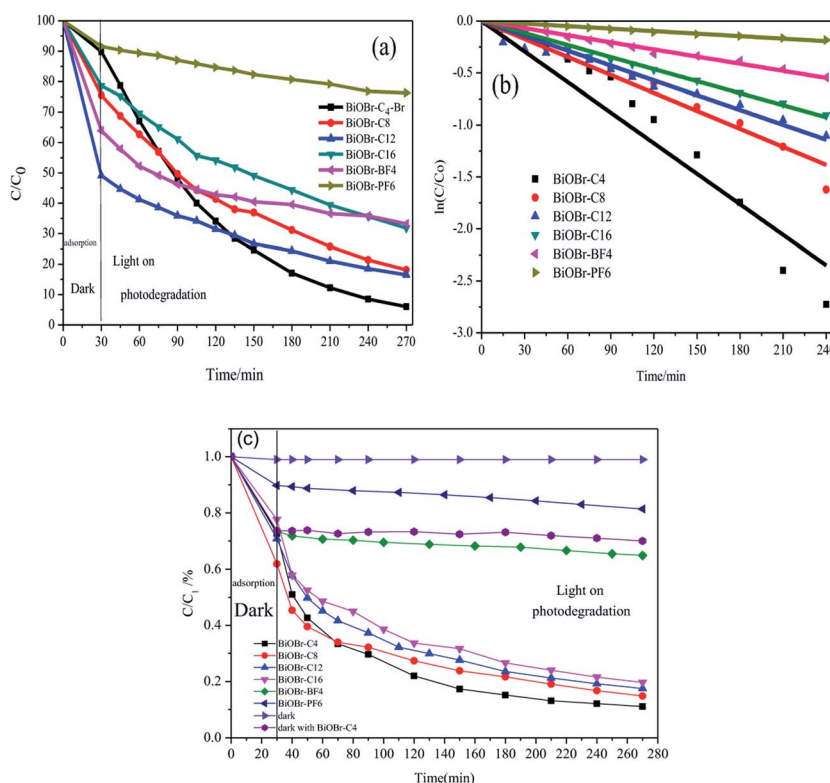

Fig. 4   (a) Photocatalytic activity and (b) pseudo-first-order reaction kinetics of BiOBr prepared by different kinds of ionic liquids for the degradation of MO. (c) Photocatalytic performance of tetracycline decomposition under visible irradiation.

the photocatalyst. Therefore, a colourless contaminant should be selected as the model pollutant to further confirm the photocatalytic activity of BiOBr. Tetracycline hydrochloride was chosen as the model pollutant in our next experiment. The photocatalytic performances of BiOBr on the degradation of tetracycline hydrochloride are exhibited in Fig. 4(c), and demonstrated the same tendency as with MO removal. According to the above results, the photocatalytic activities of BiOBr prepared *via* an IL method were confirmed. Furthermore, we showed an enhanced photocatalytic activity compared with the previously reported study,[4] which can be ascribed to the multi-reflections of the light by the hierarchical morphology.

To investigate the effects of the different types of IL-functionalized BiOBr samples, PL spectroscopy was performed and spectra are presented in Fig. 5. The intensity of the maximum emission peaks gradually decreased as the chain length of the ILs increased. Jing *et al.*[29] argued that stronger PL intensity comes from a higher concentration of oxygen vacancies, and that more efficient photocatalytic activity could be achieved with higher oxygen vacancy concentrations. The reason is that PL emission results from the surface oxygen vacancies during the photoluminescence process, while surface oxygen vacancies are favourable for the photocatalytic oxidation reaction. In Fig. 6, oxygen vacancies were tested from BiOBr-C_4-Br; the results can be inferred for BiOBr-C_8, BiOBr-C_{12} and BiOBr-C_{16} since all samples were prepared by the same procedure and the oxygen vacancies all originated from O-atoms, which derived from the reagents. Consequently, the trends exhibited by the MO degradation experiments suggested that the results of the degradation of MO were consistent with the PL results.

Electrochemical impedance spectroscopy (EIS), which can be utilized to explore the rules of the photogenerated charge carrier separation procedure, gave the Nyquist plots in Fig. 7. It was observed that the diameters of the semicircles in the plots became shorter as the chain lengths of the ILs increased. Furthermore, the radiuses of the BiOBr-BF_4 and BiOBr-PF_6 spectra were bigger than those of the other BiOBr samples. The order of the radius length was BiOBr-C_4-Br < BiOBr-C_8 < BiOBr-C_{12} < BiOBr-C_{16} < BiOBr-BF_4 < BiOBr-PF_6, which was consistent with the results of PL spectroscopy and EPR. Our PL and EPR data, and the previously reported results,[29] suggested that the PL intensity became stronger gradually as the concentration of the oxygen vacancies increased. As is known to all, oxygen
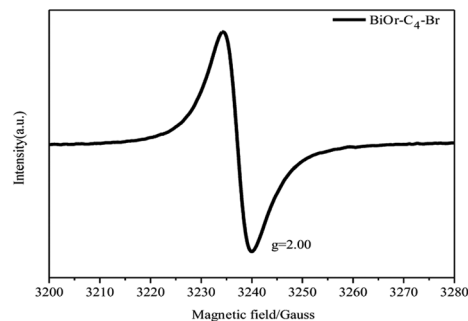

Fig. 6   EPR spectra of BiOBr-C_4-Br samples.

vacancies can trap photoelectrons to prolong the recombination time of the carriers.[30] Therefore, more electrons and holes can take part in the procedure of photocatalysis. That is to say, the BiOBr samples with smaller radiuses in EIS showed stronger PL intensity, and possessed a higher concentration of surface oxygen vacancies and better photocatalytic activity. BiOBr-C_4-Br particles had the best efficiencies in the separation of photogenerated electrons and holes. The results indicated that ILs have significant effects on the charge-transfer process and the efficiency of the interfacial charges, which led to the different photocatalytic performances of the BiOBr in terms of the degradation process.

It is remarkable and well-known that the crystal facet typically has an enormous effect on a catalyst because it may affect the particle size, the material structure, the capability for optical absorption, *etc.* Several researchers have insisted that ILs have effects on the growth of the crystal facets in synthesized materials,[31–33] including nanoplate-like BiOBr. Accidently, it was found that the proportion of (011) facets of BiOBr differed from the anions of the ILs used, as listed in Table 1. However, microflowers of BiOBr synthesized without ILs did not have varying proportions of (011) facets.[8,34] Furthermore, BiOBr microparticles were also obtained by 1-butyl-3-methylimidazolium tetrafluoroborate and 1-butyl-3-methyl-imidazole hexafluorophosphate. From the XRD results and the calculation of the proportion of (011) facets, there was an intriguing phenomenon that the ratio of the (011) facets improved as the chain lengths of the ILs increased, which was manifested in Table 1. The order of the proportion of (011)
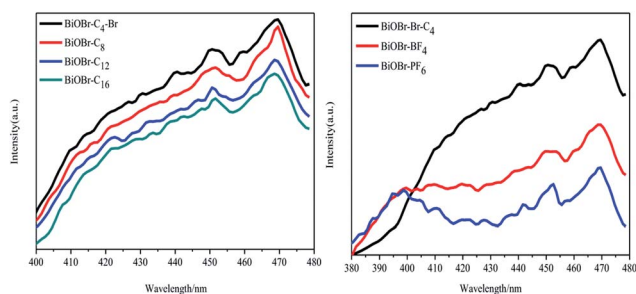

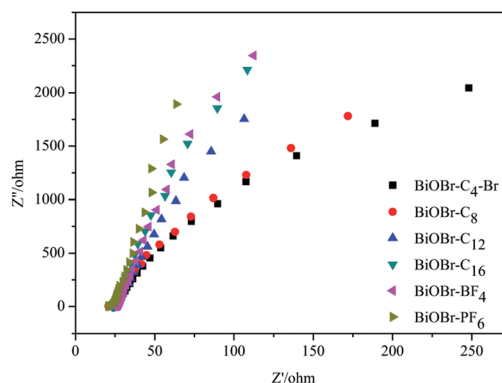Fig. 5   Photoluminescence spectra of BiOBr synthesized by different kinds of ionic liquids.

Fig. 7   Electrochemical impedance spectra for the BiOBr samples.

facets from low to rich was BiOBr-C$_4$-Br < BiOBr-C$_8$ < BiOBr-C$_{12}$ < BiOBr-C$_{16}$ < BiOBr-BF$_4$ < BiOBr-PF$_6$. The BiOBr prepared by 1-butyl-3-methylimidazolium tetrafluoroborate showed a higher proportion of the exposed (011) facets compared to the BiOBr prepared by 1-butyl-3-methylimidazolium bromide, 1-octyl-3-methylimidazolium bromide, 1-dodecyl-3-methylimidazolium bromide and 1-cetyl-3-methylimidazolium bromide. Moreover, BiOBr modified by the 1-butyl-3-methyl-imidazole hexafluorophosphate displayed the highest ratio of (011) facets. In other words, to increase the proportion of the exposed (011) facets, BiOBr should be obtained through 1-butyl-3-methylimidazolium tetrafluoroborate and 1-butyl-3-methyl-imidazolium hexafluorophosphate.

Previously, Zhang and co-workers have computed the density of states (DOS) and partial density of states (PDOS) to verify the surface states of BiOBr.[35] They showed that surface oxygen vacancies existed within all facets, except for the {011} facets. Based on the calculation of (011) facets exhibited in Table 1, it is evident that the proportion of (011) facets changed regularly (the ratio of the (011) surface increased as the chain length of the IL decreased). A possible mechanism is proposed on the basis of the previous study[29,35] and the above experimental results. As is known to all, oxygen vacancies can trap photoelectrons to prolong the recombination time of the carriers, which makes it possible to separate the electrons and holes initially. The enhancement in the photocatalytic activity of the as-prepared BiOBr can be explained by the theory illustrated in Fig. 8. When the catalysts are irradiated by light, the VB electrons of BiOBr samples are excited to the CB level, nevertheless,

the holes still remain in the VB. For BiOBr-C$_4$-Br, some of the electrons are separated by (011) facets and other surfaces from the holes. Simultaneously, other electrons and holes are accumulated on the (011) facets. When the ratio of (011) facets continuously increases, some electrons or holes can be transferred from other crystal faces to the (011) facets. The charge carriers in the (011) facets are easily recombined due to the lack of oxygen vacancies. Thus, only a few electrons and holes can participate in the photocatalytic reaction. In other words, with a decreasing proportion of (011) surfaces, some electrons or holes can efficiently migrate to other surfaces which are not (011) facets, making charge recombination more difficult. As a result, the photocatalytic activity is enhanced as the proportion of (011) facets decreases. The theory is similar to that proposed in the previous report.[36]

The recycling tests of the BiOBr-C$_4$-Br for tetracycline hydrochloride degradation under visible light were also performed to assess the stability of the samples. As exhibited in Fig. 9(a), approximately 90% of tetracycline hydrochloride could be removed in the first round and the efficiency could be retained at 75% after four runs, indicating that the sample had a good photocatalytic stability after four recycles. In addition, XRD patterns of the BiOBr-C$_4$-Br after four cycles are displayed in Fig. 9(b). No obvious change can be found before and after four cycling experiments, which suggests that the BiOBr prepared via ILs had a stable structure. From the XRD patterns of the pristine BiOBr and BiOBr after use, it can be deduced that the decrease of photocatalytic efficiency did not originate from
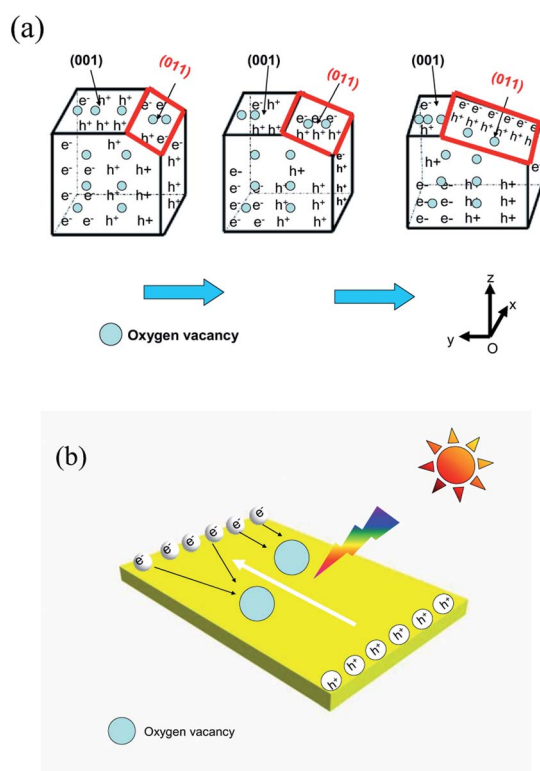

Fig. 8 Schematic illustration of BiOBr enhanced photocatalytic activity (a) by (011) facet reduction and (b) by oxygen vacancies.
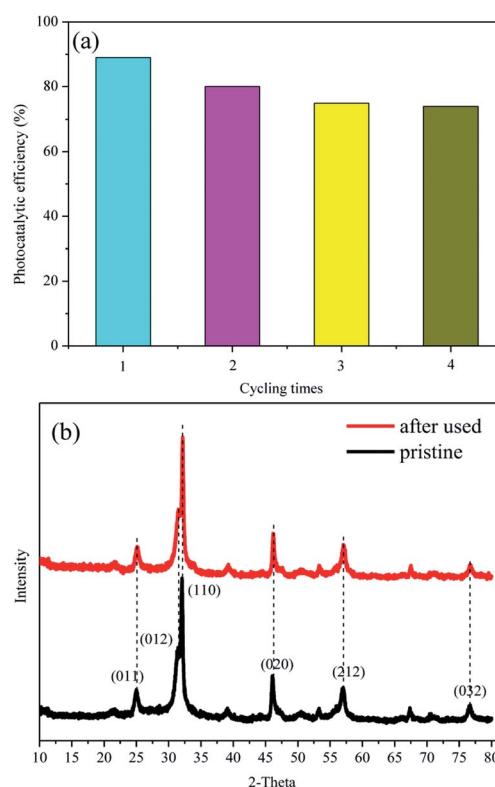

Fig. 9 (a) Recycling tests of BiOBr-C$_4$-Br and (b) XRD patterns of pristine BiOBr-C$_4$-Br and the samples after four cycles.

structure damage. We suggest that the decline in the photocatalytic activity should be attributed to the processes of recycling and washing which can cause the loss of the photocatalyst. Additionally, the adsorption capability will be decreased after several runs because chemical adsorption might have happened, which will decrease the adsorption ability of the photocatalysts. Further study is needed to confirm the types of adsorption.

4. Conclusions

In summary, hierarchical BiOBr microspheres with an average diameter of 2–4 μm have been synthesized successfully *via* a solvothermal process in the presence of imidazole ILs. The experimental results reveal that oxygen vacancies could be responsible for the enhanced visible photocatalytic activity of the as-prepared BiOBr in terms of its degradation of organic pollutants. This enhancement could be ascribed to the efficient separation of the photoelectron–hole pairs by oxygen vacancies and the variation of crystal surfaces. It is concluded that BiOBr-C_4-Br which has the lowest proportion of (011) facets shows better photocatalytic activity than the other BiOBr catalysts. This finding provides a new insight into the fabrication and design of the photocatalytic BiOBr catalysts, which could be applied for contaminant removal.

Conflicts of interest

There are no conflicts to declare.

Acknowledgements

References

1 A. Fujishima and K. Honda, *Nature*, 1972, **238**, 37–38.
2 Z. G. Zou, J. H. Ye, K. Sayama and H. Arakawa, *Nature*, 2001, **414**, 625–627.
3 S. Li, S. Hu, W. Jiang, Y. Liu, J. Liu and Z. Wang, *J. Colloid Interface Sci.*, 2017, **501**, 156–163.
4 X. Mao, F. Xie and M. Li, *Mater. Lett.*, 2016, **166**, 296–299.
5 S. Y. Song, Y. Zhang, Y. Xing, C. Wang, J. Feng, W. D. Shi, G. L. Zheng and H. J. Zhang, *Adv. Funct. Mater.*, 2008, **18**, 2328–2334.
6 H. Tong, S. X. Ouyang, Y. P. Bi, N. Umezawa, M. Oshikiri and J. H. Ye, *Adv. Mater.*, 2012, **24**, 229–251.
7 J. Di, J. Xia, H. Li, S. Guo and S. Dai, *Nano Energy*, 2017, **41**, 172–192.
8 D. Zhang, J. Li, Q. G. Wang and Q. S. Wu, *J. Mater. Chem. A*, 2013, **1**, 8622–8629.
9 Y. Fang, Y. Huang, J. Yang, P. Wang and G. Cheng, *Environ. Sci. Technol.*, 2011, **45**, 1593–1600.
10 J. Zhang, F. Shi, J. Lin, D. Chen, J. Gao, Z. Huang, X. Ding and C. Tang, *Chem. Mater.*, 2008, **20**, 2937–2941.
11 Z. T. Deng, D. Chen, B. Peng and F. Q. Tang, *Cryst. Growth Des.*, 2008, **8**, 2995–3003.
12 J. W. Wang and Y. D. Li, *Chem. Commun.*, 2003, 2320–2321.
13 J. X. Xia, S. Yin, H. M. Li, H. Xu, L. Xu and Y. G. Xu, *Dalton Trans.*, 2011, **40**, 5249–5258.
14 D. Q. Zhang, M. C. Wen, B. Jiang, G. S. Li and C. Y. Jimmy, *J. Hazard. Mater.*, 2012, **211–212**, 104–111.
15 Z. Jiang, F. Ang, G. D. Yang, L. Kong, M. O. Jones, T. C. Xiao and P. P. Edwards, *J. Photochem. Photobiol., A*, 2010, **212**, 8–13.
16 Y. C. Feng, L. Li, J. W. Li, J. F. Wang and L. Liu, *J. Hazard. Mater.*, 2011, **192**, 538–544.
17 Z. H. Ai, W. Ho, S. Lee and X. Y. Zhang, *Environ. Sci. Technol.*, 2009, **43**, 4143–4150.
18 Y. N. Wang, K. J. Deng and L. Z. Zhang, *J. Phys. Chem. C*, 2011, **115**, 14300–14308.
19 F. Caruso, *Adv. Mater.*, 2001, **13**, 11–22.
20 R. Katoh, M. Hara and S. Tsuzuki, *J. Phys. Chem. B*, 2008, **112**, 15426–15430.
21 S. j Guo, S. J. Dong and E. K. Wang, *Adv. Mater.*, 2010, **22**, 1269–1272.
22 J. Xia, J. Di, H. Li, H. Xu, H. Li and S. Guo, *Appl. Catal., B*, 2016, **181**, 260–269.
23 Z. H. Li, Z. M. Liu, J. L. Zhang, B. X. Han, J. M. Du, Y. N. Gao and T. Jiang, *J. Phys. Chem. B*, 2005, **109**, 14445–14448.
24 K. L. Ding, Z. J. Miao, Z. M. Liu, Z. F. Zhang, B. X. Han, G. M. An, S. D. Miao and Y. Xie, *J. Am. Chem. Soc.*, 2007, **129**, 6362–6363.
25 I. Yavari, A. R. Mahjoub, E. Kowsari and M. Movahedi, *J. Nanopart. Res.*, 2009, **11**, 861–868.
26 A. Taubert, *Angew. Chem., Int. Ed.*, 2004, **43**, 5380–5382.
27 X. D. Liu, J. M. Ma, P. Peng and W. J. Zheng, *Langmuir*, 2010, **26**, 9968–9973.
28 M. A. Butler, *J. Appl. Phys.*, 1977, **48**, 1914–1920.
29 L. Jing, B. Xin, D. Wang, F. Yuan, H. Fu and C. Sun, *Chem. Res. Chin. Univ.*, 2005, **26**, 111–115.
30 L. Jing, Y. Zheng and X. Li, *Chem. Res. Chin. Univ.*, 2001, **22(11)**, 1885–1888.
31 X. Zhou, Z. X. Xie, Z. Y. Jiang, Q. Kuang, S. H. Zhang, T. Xu, R. B. Huang and L. S. Zheng, *Chem. Commun.*, 2005, 5572–5574.
32 D. Zhang, G. Li, X. Yang and C. Y. Jimmy, *Chem. Commun.*, 2009, 4381–4383.
33 K. Qi, J. Yang, J. Fu, G. Wang, L. Zhu, G. Liu and W. Zheng, *CrystEngComm*, 2013, **15**, 6729–6735.
34 X. Wang, J. Yang, Y. Chen, Y. Zhang and Y. Tang, *Mater. Lett.*, 2014, **116**, 171–174.
35 H. Zhang, L. Liu and Z. Zhou, *RSC Adv.*, 2012, **2**, 9224–9229.
36 J. Yu, J. Low, W. Xiao, P. Zhou and M. Jaroniec, *J. Am. Chem. Soc.*, 2014, **136**, 8839–8842.